Photoelectron Spectroscopy and Thermochemistry of *tert*-Butylisocyanide-Substituted Cobalt Tricarbonyl Nitrosyl[†]

Zsolt Gengeliczki,[‡] László Szepes,[‡] Bálint Sztáray,[*,‡] and Tomas Baer[£]

Institute of Chemistry, Eötvös Loránd University Budapest, Hungary, H-1117 Budapest, Pázmány P. sétány 1/A, and Department of Chemistry, University of North Carolina, Chapel Hill, North Carolina 27599-3290

A new organometallic complex, $Co(CO)_2NO^tBuNC$, was synthesized and investigated by photoelectron spectroscopy (PES) and threshold photoelectron photoion coincidence (TPEPICO) spectrometry in order to determine its ionization energy as well as the bond energies in the ionic forms. The assignment of the nine peaks in the PES was based on Kohn−Sham molecular orbital energies, and an adiabatic ionization energy of 7.30 ± 0.05 eV was determined. In the TPEPICO experiment, the following 0 K onsets were determined for the various fragment ions: $CoCONO^tBuNC^+$ (8.17 ± 0.05 eV); $CoNO^tBuNC^+$ (9.01 ± 0.05 eV); and Co^tBuNC^+ (10.42 ± 0.05 eV). Because the photon source did not extend above 14 eV, we could not observe the bare Co^+ ion in the experiment. The heat of formation of the Co^tBuNC^+ ion was estimated by ab initio and DFT calculations of the $CoL^+ + {^t}BuNC \rightarrow Co^tBuNC^+ + L$ ($L = CO$, NO, NH_3, H_2O, PMe_3) substitution enthalpies.

Introduction

Organometallic complexes and their ions often dissociate in a simple sequential manner, which is very different from most organic molecules, which dissociate via competitive parallel pathways. This is because the metal−ligand bonds are generally weaker than the bonds within the ligands, and there are significant differences between the bond energies of the central metal and the various ligands. Furthermore, these weak metal−ligand bond energies and their resulting reactivity are one reason that organometallic complexes are useful as catalysts[1−3] and chemical vapor deposition (CVD) precursors.[4−12] Therefore, the metal−ligand bond energies and their thermochemistry, in general, are important in a wide range of reactions.

In the past few years, we have embarked on an experimental program to measure the metal−ligand bond energies and the thermochemistry of organometallic complexes (such as C_5H_5-$Co(CO)_2$,[13,14] $C_5H_5Mn(CO)_3$,[15] $C_6H_6Cr(CO)_3$,[16] $(C_5H_5)_2Mn$,[17] $(C_6H_6)_2Cr$,[18] $Co(CO)_3NO$,[19] $Co(CO)_2NOPR_3$,[20] where $R = CH_3$ or C_2H_5, and $C_5H_5Mn(CO)_2CX$[21] where $X = S$ or Se) by the method of threshold photoelectron photoion coincidence (TPEPICO). Because various substituents affect the chemical reactivity of the complex, it is of great interest to systematically replace one of the carbonyl ligands with various ligands to measure the effect on the metal−carbonyl bond energies and the thermochemistry of the complex. Having studied the phosphine derivatives of cobalt tricarbonyl nitrosyl,[20] we focus in this work on its isocyanide derivative, $Co(CO)_2NO^tBuNC$, in which one of the carbonyl ligands is replaced by *tert*-butyl isocyanide. The isocyanide group is a carbonyl analogue ligand, and the electron donor properties of the isocyanide ligand can be tuned by changing the alkyl group.

In the present study, we combine the results of photoelectron spectroscopy (PES) and TPEPICO in order to measure the

ionization energy, investigate the electron structure of the neutral molecule, and determine the metal−ligand bond energies in the various fragment ions. The heats of formation of many organometallic complexes, including $Co(CO)_2NO^tBuNC$, are not known. However, by measuring the photon energy required to generate the bare metal ion plus the free ligands, it is possible to use this final state as an anchor to determine the heats of formation of the neutral complex as well as all of the ion products. Because the available photon energy from our light source was not sufficiently high to observe bare cobalt ions, no state with a known heat of formation could be reached. In order to establish the heats of formation of the various fragment ions and the neutral molecule, we carried out DFT and ab initio calculations on the Co^tBuNC^+ ion. However, calculating substitution or dissociation enthalpies for transition-metal complex ions is a challenging problem. The open shell electronic structure and the presence of heavy atoms result in higher electron correlation energies and relativistic effects than those in common organic molecules. Because the available state-of-the-art extrapolation methods (e.g., G2, G3, etc.) are not optimized for transition-metal elements, their accuracy for these complexes is not guaranteed. To predict the accuracy of any quantum chemical calculation is even more difficult in the case of ions because relatively few experimental values are available for comparison. In the present study, density functional theory (DFT) and coupled cluster (CC) studies were carried out on the $CoL^+ + {^t}BuNC \rightarrow Co^tBuNC^+ + L$ ($L = CO$, NH_3, NO, PMe_3, H_2O) substitution enthalpies to establish the heat of formation of the Co^tBuNC^+ ion.

Experimental Section

Preparation of the Sample. The synthesis of a similar complex ($Co(CO)_2NO(CNC_6H_{11})$) was reported by Thorsteinson and Basolo.[22] That method was slightly modified and used to synthesize $Co(CO)_2NO(^tBuNC)$. At room temperature, ^tBuNC (2.32 g, 28.0 mmoles) was added in small portions to $Co(CO)_3NO$ (5.19 g, 30.0 mmoles) in tetrahydrofuran (50 mL)

*t*BuNC-Substituted Co(CO)₃NO

J. Phys. Chem. A, Vol. 111, No. 31, 2007 **7543**

under an inert atmosphere of nitrogen. The reaction mixture was stirred for 3 h before the solvent and the excess reactant were removed at reduced pressure. The product was isolated as a dark-red liquid with a yield of 80%. Because of its presumed sensitivity to air and water, it was stored under an inert atmosphere at -25 °C until used in the experiments.

The $Co(CO)_3NO$ and ^tBuNC were purchased from Strem Chemicals and Sigma$-$Aldrich, respectively, and were used without further purification. The tetrahydrofuran was dried over CaH_2, refluxed with sodium and benzophenone, and then distilled under nitrogen.

Ultraviolet Photoelectron Spectroscopy (UPS). HeI photoelectron spectra were recorded on an ATOMKI ESA 32 instrument in Budapest. The instrument, which was operated with a resolution of 30 meV, has been described elsewhere.[23] The sample was introduced into the ionization chamber via a direct inlet system at room temperature. Argon was used as an internal standard, and the spectra were calibrated against the Ar $^2P_{1/2}$ and $^2P_{3/2}$ peaks. Besides determining vertical ionization energies to study the electronic structure of the complex, the HeI PES was also used to determine the adiabatic ionization energy, which is essential in the analysis of the TPEPICO experiments (see below), and to obtain insight into the electronic structure of neutral $Co(CO)_2NO^tBuNC$.

Threshold Photoelectron Photoion Coincidence (TPEPICO). The details of the TPEPICO spectrometer have been described previously.[24] The sample had a sufficiently high vapor pressure to permit its introduction into the ionization region at room temperature through a hypodermic needle. The sample was ionized with vacuum ultraviolet (VUV) light from a H_2 discharge lamp dispersed by a 1 m normal incidence vacuum monochromator. The VUV wavelengths were calibrated using the hydrogen Lyman-α resonance line. The ions and the electrons were extracted in opposite directions with an electric field of 20 V/cm. The electrons traveled 6.75 mm through this region before they were accelerated to about 70 V by the second acceleration region into the velocity-focusing flight tube[25] of 13 cm length. Electrons with zero velocity perpendicular to the extraction voltage were focused to a spot at the end of the flight tube, whereas the energetic electrons were focused onto rings around this central spot with radii proportional to their initial velocity perpendicular to the extraction axis. In the center, the electrons were detected by a Channeltron electron detector with a 1 mm cone, while the electrons with a certain perpendicular velocity were detected by a Chevron stack of microchannel plates with a center hole for the above-mentioned Channeltron. Assuming that the hot electron signal in a ring around the central spot was proportional to the hot electron contribution in the central spot, a weighed fraction of the outer ring signal could be subtracted from the central electrode signal, thereby correcting the TPEPICO TOF mass spectrum for this contribution of initially energetic ("hot") electrons.[26]

After exiting the 5 cm long first acceleration region, the ions entered the 38 cm long drift region, which ended in a 24 cm long reflectron where the ions were reflected by a voltage of 141 V. After traversing the second, 35 cm long drift region, they were detected with a multichannel plate (MCP) detector. The electron and ion signals served as start and stop pulses for measuring the ion time-of-flight (TOF), and the TOF for each coincidence event was stored on a multichannel pulse height analyzer. Because both the center and the ring electron signals served as start signals, two TOF distributions were obtained at each photon energy. TOF distributions were obtained in 6$-$48 h depending on the signal intensity and the desired spectrum

quality. The weighed fraction of the TOF distribution generated by the ring electrode signal was subtracted from the center electrode signal to correct for the hot electron contribution. In order to analyze the shape of the TOF distributions, the ring distribution was subtracted from the center TOF distribution point by point using a 10 point interpolation scheme.

The PEPICO spectra were used for two purposes. First, the fractional abundances of the parent and the daughter ions were measured as a function of the photon energy (breakdown curve). Second, ion decay rates were extracted from asymmetric TOF distributions of the daughter ion signal. This asymmetry is the result of slowly dissociating (metastable) ions dissociating in the 5 cm acceleration region, resulting in a time-of-flight between the parent and the daughter ion's flight time. In addition to this asymmetry, a Gaussian-shaped peak appeared between the daughter ion and the parent ion signal. This peak is the result of metastable ions dissociating in the field-free region between the acceleration region and the reflectron. These two types of information were used together in the data analysis as described in a later section in detail.

Quantum Chemical Calculations

Quantum chemical calculations were carried out in order to help the assignment of the photoelectron spectrum, determine the vibrational frequencies of the neutral molecule and the various fragment ions, and to establish the thermochemistry of the $Co(CO)_x(NO)_y^tBuNC^+$ system. On the basis of the desired accuracy of the calculated physical property, we used different levels of theory and basis sets.

Ionization Energies The application of Koopmans's theorem to determine vertical ionization energies, which equates the negative of the Hartree$-$Fock orbital energies with the ionization energy, is known to be subject to considerable error. As shown by Baerends et al.[27$-$32] and tested in our recent studies,[33,34] negatives of Kohn$-$Sham orbital energies can be taken as approximate vertical ionization energies. Although these orbital energies are usually lower than the experimental ionization energies, they differ systematically from the correct values. In the present study, the first vertical ionization energy was determined at the same level of theory from the difference in the ground-state energy of the ion at the neutral molecule's geometry and of the neutral molecule. The negatives of the Kohn$-$Sham orbital energies were then shifted so that the negative of the HOMO energy matched with this ΔDFT-calculated vertical ionization energy. This method provides a reliable assignment in the case of transition-metal complexes, as shown in our recent study.[34] In the calculations outlined above, Becke's three parameter hybrid functional[35] (B3) was combined with the correlation functional of Lee, Yang, and Parr[36] (LYP) and utilized with Ahlrichs's TZVP[37] basis set.

Vibrational Frequencies Vibrational frequencies of various species were needed for the calculation of the internal energy distribution of the neutral $Co(CO)_2NO(^tBuNC)$, for the calculation of the RRKM rate constants, and for the product energy distribution calculations. These frequencies were also used in the conversion of the heats of formation from 0 to 298 K (see below). Because, as it is discussed later, the four lowest frequencies of the transition states were scaled to fit to the experimental dissociation rates, the accuracy of the individual frequencies were not a real concern. Thus, we have used only one level of theory with one (sufficiently large) basis set. All of the calculations were carried out at the DFT level using the B3LYP functional[35,36] and 6-31++G**[38] basis set for the neutral and dissociating ions and the smaller LanL2DZ basis set[39] for

the transition states. In these calculations, the singlet spin state was found to be lowest for the neutral precursor, and a doublet state was found for the dissociating ionic species and triplet state for the Co^{t}BuNC$^+$ ion.

Because these dissociations proceed with no reverse barrier, the transition states do not correspond to a critical point on the potential energy surface. To approximate the structure and vibrational frequencies of the transition states, the metal–carbonyl bond distances of the leaving carbonyl groups were fixed at 4.0 Å, and the energy was optimized with respect to the remaining coordinates. The distance of 4.0 Å was suggested by previous variational transition-state theory (VTST) calculations of another cobalt–carbonyl complex.[13] In the case of the third transition state, namely, the [CoNO(^{t}BuNC)]$^+$ with an elongated Co–NO distance, the quantum chemical calculations did not converge. Consequently, the precursor ion frequencies were used as estimates for the frequencies of the third transition state. The Co–NO stretching mode obtained from the calculation (558 cm^{-1}) for CoNO(^{t}BuNC)$^+$ was assigned as the critical frequency for the dissociation step and thus deleted. Furthermore, the transitional vibrational modes were identified, and those frequencies were lowered and then fitted, as explained later. In the RRKM calculations of the dissociation rates, the TS frequencies were used as the starting point for fitting the experimental dissociation rate curves. The lowest four frequencies of the transition states, which turn into product rotations and translations, were optimized in order to fit the calculated TOF distributions and breakdown diagrams to the experimentally measured data. These harmonic vibrational frequencies along with the details of the data analysis can be viewed in the Supporting Information.

Thermochemical Data. Because the available photon energy was not enough to produce the bare cobalt ion, no product state whose energies are well-known was reached. The highest accessible energy channel was the production of the Co^{t}BuNC$^+$ ion. To establish the heats of formation of the various ionic species and the neutral molecule, the heat of formation of the Co^{t}BuNC$^+$ ion was estimated by ab initio and DFT calculations of the following substitution enthalpies

$$CoL^+ + {}^tBuNC \rightarrow Co^tBuNC^+ + L \qquad (1)$$

Isodesmic reactions have been shown to be useful in determining unknown heats of formation in previous studies on other organoelement molecules.[40,41] However, no heat of formation of any CoRNC$^+$ ion is known; therefore, real isodesmic reactions could not be included in this study. Instead, L = CO, NH$_3$, NO, PMe$_3$, and H$_2$O ligands, which share some of the important properties of the ^{t}BuNC ligand in the formation of complexes, were used.

In one type of the calculations, the 6-311++G(2df,p)[42–44] basis set was used on all of the atoms in the ions and neutral ligands, while in the second type of the calculations, relativistic effects arising from the interaction of the heavy nuclei and the inner electrons were taken into account by utilizing Christiansen's CRENBL basis set with the effective core potential (ECP)[45,46] on the cobalt atom and Dunning's correlation-consistent pVTZ basis set[47] on the ligand atoms.

At the DFT level, the B3LYP functional was combined with the above-mentioned basis sets. The wave functions were checked for internal instabilities by using Pople's method.[48,49] The obtained equilibrium geometries were verified by the absence of imaginary vibrational frequencies. These frequencies were also used to calculate the zero point energy corrections.
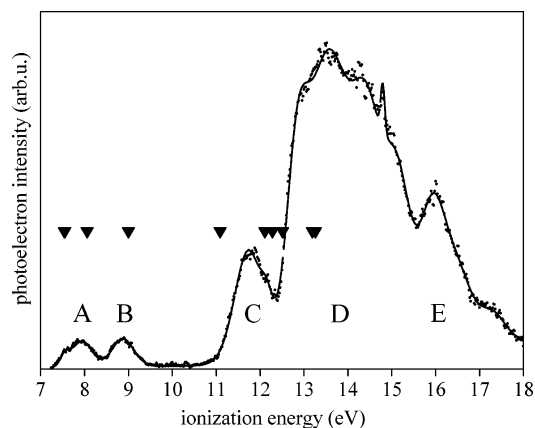
Figure 1. HeI photoelectron spectrum of Co(CO)$_2$NO(^{t}BuNC) with the calculated (B3LYP/TZVP) ionization energies.

In the ab initio calculations, the geometries were obtained with Møller–Plesset-partitioned second-order perturbation theory (MP2)[50] using the above-described basis sets and tested in the same manner. Coupled cluster calculations with single, double, and perturbative triple excitations[51] were carried out on the stable geometries. The enthalpies of substitutions described by eq 1 were then derived from the CCSD(T) energies, and zero point energy corrections were calculated from the MP2 vibrational frequencies.

The discussion of the derived heats of formation can be found in the Data Analysis section. Details about the quantum chemical calculations (zero point energy corrections and substitution enthalpies) can be found in the Supporting Information. All of the quantum chemical calculations were carried out with the Gaussian03, revisions B.04[52] and D.01,[53] code.

Experimental Results

UPS. The recorded HeI PES is shown in Figure 1. The determination of the adiabatic ionization energy is quite difficult unless the bands are vibrationally resolved, which is rarely the case for polyatomic molecules. Thus, the adiabatic ionization energy has a larger uncertainty than the vertical ionization energy, which is simply the first peak position of the HeI PES. The adiabatic ionization energy was estimated to be 7.30 ± 0.05 eV.

The HeI PES contains five partly overlapping bands in the energy range of 7–18 eV. To extract the vertical ionization potentials, pseudo-Voigt-shaped peaks were fitted to the measured spectrum. The broad band starting at approximately 13 eV is unresolvable, which is why the experimental vertical ionization energies, with the calculated ionization energies and the characters of the orbitals, are listed only up to 13 eV. The interpretation of the spectrum is greatly aided by analogy with the assigned HeI photoelectron spectra of Co(CO)$_3$NO[54–56] and Co(CO)$_2$NOPMe$_3$.[33] The assignments are also supported by DFT (B3LYP/TZVP) calculations.

TPEPICO. TOF mass spectra of Co(CO)$_2$NO(^{t}BuNC)$^+$ were collected in the photon energy range of 7.5–12 eV. The collection and analysis of data were rendered more difficult by the relatively low stability of the sample. Solid decomposition products in the sample container and unexpected peaks in the TOF mass spectra were observed after some time. Later, during the analysis, the peaks corresponding to these impurities were identified and removed from the spectra. Typical time-of-flight distributions without hot electrons (see the Experimental Section) are shown in Figure 2a–c for all three dissociation steps. The experimental data are plotted, while the solid lines show the fitted TOF distributions, as discussed in the Data Analysis

*t*BuNC-Substituted Co(CO)₃NO

*J. Phys. Chem. A, Vol. 111, No. 31, 2007* **7545**
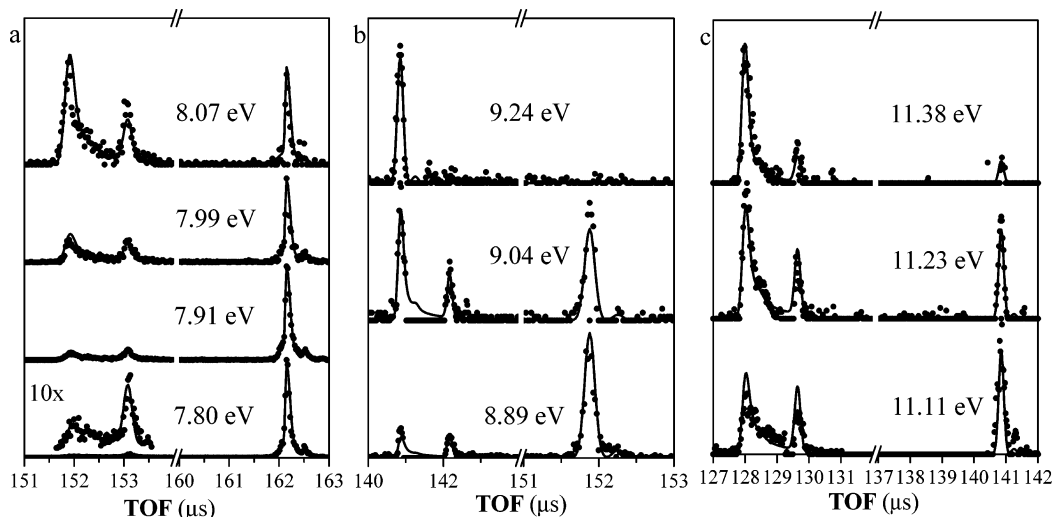
Figure 2. Ion TOF distributions at selected photon energies. Points are the experimental data, while the solid lines show the calculated TOF distributions, as described in the Data Analysis. (a) The first carbonyl loss: the asymmetric peak between 151.5 and 153.5 μs is assigned to the CoCONO(CN^{t}Bu)$^+$ ion, while the symmetric peak at 162.2 μs belongs to the parent ion, Co(CO)₂NO(CN^{t}Bu)$^+$. (b) The second carbonyl loss: the first peak at about 140.9 μs is due to the second daughter ion, CoNO(CN^{t}Bu)$^+$, while the second peak at 151.9 μs belongs to CoCONO(CN^{t}Bu)$^+$. (c) The nitrosyl loss from CoNO(CN^{t}Bu)$^+$: the first peak between 127.7 and 130.1 μs corresponds to Co(CN^{t}Bu)$^+$, while the right-hand side peak is due to CoNO(CN^{t}Bu)$^+$. The sharp peaks on the right-hand side of the asymmetric daughter ion peaks are due to dissociation between the first acceleration region and the reflectron and, thus, are most abundant at low photon energies.

section. Below the photon energy of 8.5 eV, the two peaks correspond to the molecular ion, Co(CO)₂NO(CN^{t}Bu)$^+$ at 162.2 μs, and its daughter ion, CoCONO(CN^{t}Bu)$^+$ at 151.9 μs. At photon energies between 8.5 and 9.5 eV, the two peaks are due to CoCONO(CN^{t}Bu)$^+$ and its dissociation product, CoNO(CN^{t}Bu)$^+$ at 140.9 μs. Finally, at photon energies above 10.5 eV, we observe only CoNO(CN^{t}Bu)$^+$ and its daughter ion, Co(CN^{t}Bu)$^+$ at 128.0 μs. The maximum available photon energy in the instrument is about 14 eV, which is not sufficient to remove the *tert*-butyl isocyanide ligand from the cobalt ion.

As shown in Figure 2a–c, the daughter ion TOF distributions are asymmetric, and the so-called drift peaks can be observed at energies close to their respective appearance energies. This indicates that the ions dissociate while traveling in the acceleration region or in the first drift region of the ion optics. If an ion dissociates in the acceleration region, its final velocity as it enters the drift region will be larger than that of the parent ion but less than that of a rapidly produced daughter ion. Thus, the total flight time of these slowly produced ions falls between that of the parent ion and that of the rapidly produced daughter ion. Because there is a distribution of lifetimes at a given dissociation rate, a quasi-exponential shape of the time-of-flight peak is observed. The decay rate can be extracted from the analysis of the peak shapes. Similarly, if an ion dissociates in the drift region, its final velocity as it leaves the reflectron will be larger than that of the parent ion and less than that of a daughter ion produced in the acceleration region. However, the peak due to the ions produced in the drift region is not asymmetric since all of these ions are accelerated to the same velocity in the reflectron.

Figure 3 shows the breakdown diagram of the dissociation of Co(CO)₂NO(^{t}BuNC)$^+$. The fractional abundances of the molecular ion and the fragment ions are plotted as a function of the photon energy. The points are the experimentally determined ratios after the hot electron subtraction, while the solid lines show the results of the RRKM simulations. One of the most interesting features of this plot is the slope of the breakdown curves at the crossover points. In the case of the first dissociation, Co(CO)₂NO(CN^{t}Bu)$^+$ → CoCONO(CN^{t}Bu)$^+$ + CO, the breakdown of the parent ion abundance is quite steep, indicating a narrow distribution of the ion internal energy. The
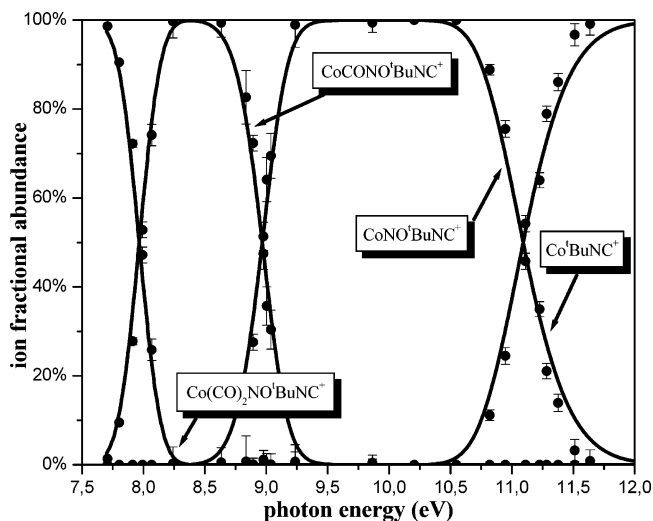
Figure 3. Breakdown curves of the two carbonyl and the nitrosyl losses. The points are the experimental data, while the solid lines are the simulated curves, as discussed in the text.

second and the third crossovers, corresponding to the carbonyl loss from CoCONO(CN^{t}Bu)$^+$ and to the nitrosyl loss from CoNO(CN^{t}Bu)$^+$, are wider, indicating a wider distribution of ion internal energies.

Data Analysis

UPS. The HeI spectrum of Co(CO)₂NO^{t}BuNC is shown in Figure 1. The assignment can be based on the similar spectra of Co(CO)₃NO and Co(CO)₂NOPMe₃.[33] The first two bands (A and B in Figure 1) in the region of 7–10 eV are expected to be the result of the ionization of orbitals that have substantial metal d character and can be regarded as π-type backbonding orbitals formed by the d orbitals of the metal center and the π* orbitals of the ligands. These two bands are followed by a peak (C between 11 and 12 eV after a wide Franck–Condon gap) that can be assigned to the ionization of molecular orbitals regarded as a bond between the cobalt atom and the ^{t}BuNC ligand and orbitals localized on the ligand. The unresolvable

TABLE 1: Experimental and Calculated Vertical Ionization Energies (eV) of Co(CO)$_2$NO(^{t}BuNC)

	Co(CO)$_2$NO^{t}BuNC		Co(CO)$_3$NO^b	
	B3LYP			
exptl	TZVP^a	MO character	exptl	MO character
7.65	7.54	Co$-$NO(π*)	8.75	Co$-$CO(π*)
7.95	8.06	Co$-$[CO(π*),NO(lp)]	9.11	Co$-$NO(π*)
8.88	9.00	Co$-$[CO(π*),NO(π*)]	9.82	Co$-$NO(π*)
11.74	11.09	Co^{t}BuNC(π)		
12.17	12.11	localized on ^{t}BuNC ligand		
	12.28	localized on alkyl		
	12.51	Co^{t}BuNC(lp)		
12.83	13.19	localized on ligands	14.14	Co$-$CO(σ)

^{a} Negatives of Kohn$-$Sham orbital energies are shifted. See details in text and ref 34. ^{b} Taken from ref 33.

broad band (D) with an onset at 13 eV is probably due to the ionization of the bonds between the metal center and its various ligands and orbitals localized on the ligands. This qualitative assignment is supported by the Kohn$-$Sham orbital energies (B3LYP/TZVP), as shown in Table 1.
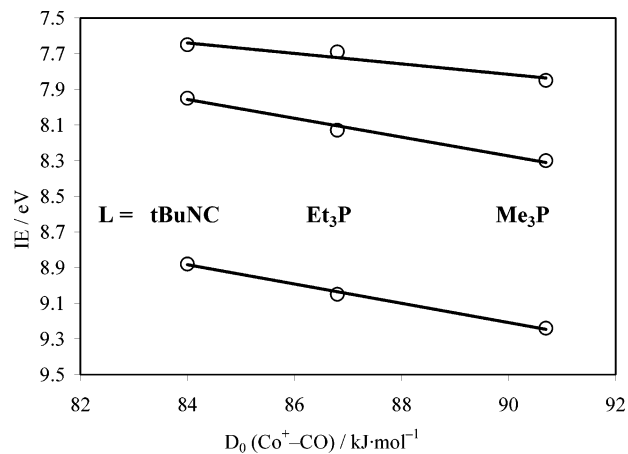
The ionization energies can be compared to those of Co-(CO)$_3$NO (Table 1). The replacement of a carbonyl group in the Co(CO)$_3$NO with the isocyanide ligand leads to the destabilization of molecular orbitals with significant metal d character. Derived from the three lowest ionization energies, the destabilizations are 1.10, 1.16, and 0.94 eV, respectively. As a result of its good electron donor capability, ^{t}BuNC increases the electron density on the metal center. This leads to the destabilization of the molecular orbitals, which are the results of the interaction between the filled metal d metal orbitals and the LUMOs of the nitrosyl and carbonyl ligands. Therefore, the electron donor capability, which can be measured with the change of the ionization potentials, can have a direct effect on the metal$-$ligand interaction.

If one compares the metal d orbital energies to those in the previously studied trialkylphosphine-substituted Co(CO)$_3$NO complexes, the ionization energies in the present complex fall between the values obtained for the triethylphosphine and the tripropylphosphine complexes. This suggests that the ^{t}BuNC ligand is a stronger electron donor than PEt$_3$ and weaker then PPr$_3$.

TPEPICO. The reaction mechanism for decomposition of the Co(CO)$_2$NO(^{t}BuNC)$^+$ ions with increasing internal energy involves the sequential loss of two carbonyl and one nitrosyl group in reactions 2 $-$ 4

$$Co(CO)_2NO(^tBuNC)^+ \rightarrow CoCONO^tBuNC^+ + CO \quad (2)$$

$$CoCONO(^tBuNC)^+ \rightarrow CoNO^tBuNC^+ + CO \quad (3)$$

$$CoNO(^tBuNC)^+ \rightarrow Co^tBuNC^+ + NO \quad (4)$$

The extraction of thermochemical data and bond energies from the experimental results requires an analysis of dissociation rates in terms of the ion internal energy distribution. Detailed descriptions of the TPEPICO data analysis have been discussed in earlier papers.[13,15$-$20] Briefly, the ion TOF distributions and the breakdown diagram can be calculated using the following information: the thermal energy distribution of the neutral Co-(CO)$_2$NO^{t}BuNC, the internal energy distribution of the dissociating ions, the ionization energy, the ion TOF parameters (acceleration electric fields and the acceleration and drift distances), and the transition-state vibrational frequencies. RRKM calculations[57,58] were performed to determine the rate constants for the three unimolecular dissociation steps of the Co(CO)$_2$NOPR$_3$$^+$ ion. (The $k(E)$ plots can be accessed in the

Figure 4. The Co(d) ionization energies in the Co(CO)$_2$NOL (L = PMe$_3$, PEt$_3$, ^{t}BuNC) complexes versus the 0 K Co$-$CO dissociation energies in their molecular ions. The change in the ionization energies is a good measure of the electron donor capability of the L ligands. For data on the phosphine complexes, see refs 20 and 33.

Supporting Information.) The following variable parameters were adjusted until the best fit was obtained: the dissociation limits and the four lowest TS vibrational frequencies. The calculations were carried out minimizing the error between the experimental and calculated TOF distributions and the break-down diagram. The best fit to both the TOF distributions and the breakdown curves was obtained with the 0 K appearance energies for CoCOCONO^{t}BuNC$^+$, CoNO^{t}BuNC$^+$, and Co^{t}BuNC$^+$ of 8.17, 9.01, and 10.42 eV, respectively. All appearance energy values have uncertainties of 0.05 eV, as discussed below. It is important to point out that, to a first approximation, the determination of each onset is independent of the previous one because, in each case, we begin from the neutral parent molecule so that the error bars do not increase with each subsequent loss of a ligand. The simulated time-of-flight distributions and breakdown curves are shown as solid curves in Figures 2a$-$c and 3, respectively.

The uncertainties in the derived parameters were studied by fixing the lowest four transition-state frequencies at various values and carrying out the fitting procedure outlined above. This scheme simulates looser and tighter transition states, thereby altering the $k(E)$ rate curves. It was found that obtaining a good fit to the breakdown curves was possible when changing the lowest four frequencies by $\pm 50\%$, but the quality of the TOF distributions got significantly worse. This is because the quasi-exponential shape of the asymmetric daughter ion distributions depends on the absolute dissociation rate, whereas the breakdown diagram depends only on the ratios of the rate constants. The optimized appearance energies change by ± 0.05 eV with the altered transition-state frequencies given above, which suggests an error bar of ± 0.05 eV for these parameters.

From the appearance energies, the following two Co$-$CO and one Co$-$NO bond energies can be obtained for the ions dissociating during the TPEPICO experiment: (^{t}BuNC)Co-(CO)$_2$NO$^+$, 84 $\pm$ 7 kJ·mol^{-1}; (^{t}BuNC)CoCONO$^+$, 81 $\pm$ 7 kJ·mol^{-1}; (^{t}BuNC)CoNO$^+$, 136 $\pm$ 7 kJ·mol^{-1}.

Correlation between Cobalt$-$Carbonyl Bond Energies and MO Energies The metal$-$carbonyl and metal$-$nitrosyl bonds are considered to be the sum of a σ-type and a π-type bond. The former is the result of the interaction between the HOMO(σ*) of the ligands and the vacant d orbitals of the metal, while the latter is the result of the interaction between the LUMO(π*) of the ligands and the occupied metal d orbitals. Therefore, a good electron donor ligand that is able to increase the electron density on the metal center can have a direct impact

*t*BuNC-Substituted Co(CO)₃NO

J. Phys. Chem. A, Vol. 111, No. 31, 2007 **7547**

TABLE 2

a. 0 K Heats of Formation of the [Co^{t}BuNC]$^+$ Ion (kJ·mol^{-1}) Derived from the
CoL$^+$ + ^{t}BuNC → Co^{t}BuNC$^+$ + L Reaction Enthalpies Obtained via Ab Initio and DFT Calculations

	ΔH_f(Co^{t}BuNC$^+$)$_{g,0K}$			
	B3LYP		CCSD(T)//MP2	
	basis set			
L	6-311++G(2df,p)	CRENBL(Co) cc-pVTZ(H, C, N, P, O)	6-311++G(2df,p)	CRENBL(Co) cc-pVTZ(H, C, N, P, O)
CO	986.4	984.8	959.8	990.1
NO	970.7	961.7	1068.1	1010.1
NH₃	1006.1	1006.7	1048.9	1009.9
PMe₃	1016.8		988.0	1006.0
H₂O	995.6	992.3	1035.9	997.3
average/SD	995.1 ± 17.8	986.4 ± 18.8	1020.1 ± 44.9	1002.7 ± 8.7

b. Reliability of the Calculated Heats of Formation.

ΔH_f(CoL$_1^+$)$_{g,0K}$ derived from CoL$_1^+$ + L$_2$ → CoL$_2^+$ + L$_1$ reaction enthalpies
CCSD(T)/CRENBL(Co), cc-pVTZ(H,C,N,P,O)//MP2/CRENBL(Co), cc-pVTZ(H,C,N,P,O)L$_1$

	L$_1$					
L$_2$	CO	NO	NH₃	PMe₃	H₂O	
CO		1073.3	913.9	814.1	776.6	
NO	916.4		933.9	834.1	796.6	
NH₃	916.1	1093.1		833.8	796.4	
PMe₃	912.3	1089.2	929.8		792.5	
H₂O	903.6	1080.5	921.1	821.3		
average/SD	912.1 ± 6.0	1084.0 ± 8.9	924.7 ± 8.9	825.8 ± 9.8	790.5 ± 9.5	
exptl	896.4 ± 7	1093.3 ± 7	933.6 ± 8.7	830 ± 12	783.8 ± 5.9	**average**
ave. − exptl	+15.7	−9.3	−8.9	−4.2	+6.7	0.0

on the metal−ligand bond energies by strengthening the π- and weakening the σ-type interaction. To see the net result of the two opposite effects, the vertical ionization energies of the neutral Co(CO)₂NOL (L = PMe₃, PEt₃, ^{t}BuNC) molecules were plotted in Figure 4 against the Co−CO bond energies in their molecular ions. A linear correlation between the Co(d) IEs and the 0 K Co−CO dissociation energies is clearly evident. The negative slopes suggest that the better electron donor capability of the ligands results in a weaker Co−CO bond. We conclude that the σ-type interaction between the metal center and the carbonyl ligands plays a more important role in the formation of the bond than the π-type back donation of the electrons from the metal to the ligands. This is supported by the fact that the nitrosyl ligand, which is assumed to donate three electrons to the metal center was found to be approximately 50% more strongly bound than the carbonyl ligand that donates only two electrons.[19] It is also interesting to point out that the PR₃ (R = Me, Et)[20,33] and the ^{t}BuNC ligands, which are thought to be mostly σ donors and only weak π acceptors, form a much stronger bond with the cobalt center than the carbonyl ligands in each ionic species.

Heat of Formation of the Co^{t}BuNC$^+$ Ion. Substitution enthalpies were calculated for the ligand substitution reactions between the CoL$^+$ (L = CO, NO, NH₃, PMe₃, H₂O) and Co-^{t}BuNC$^+$ ions

$$\Delta_r H_{g,0K} = H_{0K}(\text{Co}^t\text{BuNC}^+) - H_{0K}(^t\text{BuNC}) - $$
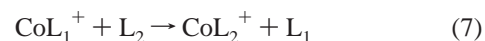$$H_{0K}(\text{CoL}^+) + H_{0K}(\text{L}) \quad (5)$$

where H_{0K} is the zero point energy-corrected electronic energy obtained in ab initio or DFT calculations. The heat of formation of the Co^{t}BuNC$^+$ ion can be derived from the substitution enthalpy

$$\Delta_f H_{g,0K}(\text{Co}^t\text{BuNC}^+) = \Delta_r H_{g,0K} + \Delta_f H_{g,0K}(^t\text{BuNC}) + $$
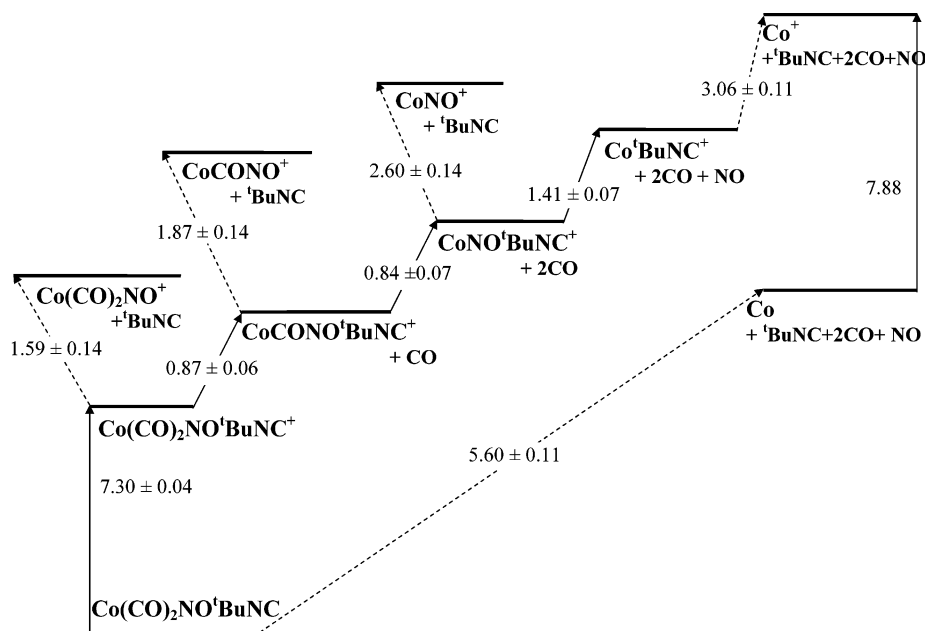$$\Delta_f H_{g,0K}(\text{CoL}^+) - \Delta_f H_{g,0K}(\text{L}) \quad (6)$$

where $\Delta_f H_{g,0K}$ is the experimental 0 K heat of formation. $\Delta_f H_{g,0K}(\text{CoCO}^+) = 896.4 ± 7$ kJ·mol^{-1}, $\Delta_f H_{g,0K}(\text{CoNO}^+) = 1093.3 ± 7$ kJ·mol^{-1}, $\Delta_f H_{g,0K}(\text{CoPMe}_3^+) = 830 ± 12$ kJ·mol^{-1}, and $\Delta_f H_{g,0K}(^t\text{BuNC}) = 77.2 ± 3.7$ kJ·mol^{-1} were taken from our earlier studies,[19,20,59] while $\Delta_f H_{g,0K}(\text{CoNH}_3^+) = 933.6 ± 8.7$ kJ·mol^{-1} and $\Delta_f H_{g,0K}(\text{CoH}_2\text{O}^+) = 783.8 ± 5.9$ kJ·mol^{-1} were derived from the heats of formation of Co$^+$ (1183.9 ± 1.0 kJ·mol^{-1}),[60] NH₃ (−38.95 ± 0.35 kJ·mol^{-1}),[61] and H₂O (−238.92 ± 0.04 kJ·mol^{-1})[61] and the bond dissociation energies of CoNH₃$^+$ ($D_{0K} = 211.3 ± 8.7$ kJ·mol^{-1})[62] and CoH₂O$^+$ ($D_{0K} = 161.1 ± 5.8$ kJ·mol^{-1}).[63]

The calculated heats of formation of the Co^{t}BuNC$^+$ ion, obtained with different methods, can be found in Table 2a. In the case of the DFT method, the use of the effective core potential shifts the average heat of formation from 995.1 to 986.4 kJ·mol^{-1}, and the standard deviation of the different heats of formation increases from 17.8 to 18.8 kJ·mol^{-1}. The effect of the ECP is more obvious in the case of the CCSD(T) calculations. The average heat of formation is shifted by 17.4 kJ·mol^{-1} from 1020.1 to 1002.7 kJ·mol^{-1}, and the standard deviation of the individual values decreases from 44.9 to 8.7 kJ·mol^{-1}. If the standard deviations are taken as uncertainties of the average heats of formation, one can see that the 1002.7 ± 8.7 kJ·mol^{-1} range obtained at the CCSD(T) level with the CRENBL ECP basis set is included in all of the ranges obtained with the other methods and basis sets. This indicates that the most precise value provided by the utilized methods might be 1002.7 ± 8.7 kJ·mol^{-1}.

The uncertainty in the above-derived $\Delta_f H_{g,0K}(\text{Co}^t\text{BuNC}^+) = 1002.7 ± 8.7$ kJ·mol^{-1}, however, is rather the precision of the method than its accuracy. One approach to testing its accuracy is to use the same approach to derive the heats of formation of the other CoL$^+$ (L = CO, NO, NH₃, PMe₃, H₂O) ions from the

$$\text{CoL}_1^+ + \text{L}_2 \rightarrow \text{CoL}_2^+ + \text{L}_1 \quad (7)$$

(L$_1$, L$_2$ = CO, NO, NH₃, PMe₃, H₂O) reaction enthalpies, for

Figure 5. Thermochemistry of the Co(CO)$_2$NO^{t}BuNC system. Ionization energies and bond energies are given in eV with their uncertainties. Dashed lines indicate derived dissociation energies, and solid lines indicate experimental values.

TABLE 3: Auxiliary, Estimated, and Derived Thermochemical Data (in kJ·mol^{-1})

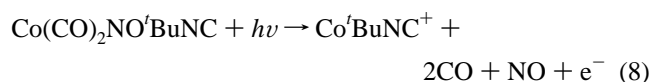|	D_0 (Co$^+$–L)	$\Delta_f H°_0$	$\Delta_f H°_{298}$	$H°_{298} - H°_0$
Co(CO)$_2$NO^{t}BuNC		-141 ± 10	-166 ± 10	46.2
Co(CO)$_2$NO^{t}BuNC$^+$	84 ± 7 (L = CO)	564 ± 11	541 ± 11	49.5
	154 ± 13 (L = ^{t}BuNC)			
CoCONO^{t}BuNC$^+$	81 ± 7 (L = CO)	762 ± 11	738 ± 11	43.0
	181 ± 14 (L = ^{t}BuNC)			
CoNO^{t}BuNC$^+$	136 ± 7 (L = NO)	956 ± 11	931 ± 11	35.4
	251 ± 14 (L = ^{t}BuNC)			
Co^{t}BuNC$^+$	295 ± 10 (L = ^{t}BuNC)	1003 ± 9	977 ± 9	27.0
Co^{+a}		1183.9 ± 1.0		
Co^a		423.5 ± 1.0		4.771
CO^a		-113.81 ± 0.17		
NO^a		89.77 ± 0.17		
^{t}BuNC^b		-113.9 ± 3.7	-88.1 ± 5	21.9

^{a} See ref 60. ^{b} See ref 59.

which the experimental values are known. These heats of formation are listed in Table 2b. It is evident that, except for the case of CO, the other four heats of formation have average values whose error limits nicely encompass the difference between the experimental and calculated values and that the average error is on the order of about 9 kJ·mol^{-1}. On the basis of these statistics, we suggest a 0 K Co^{t}BuNC$^+$ ion heat of formation of 1002.7 ± 8.7 kJ·mol^{-1}.
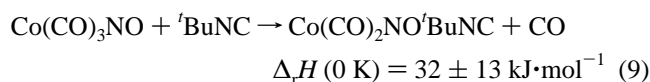
Thermochemical Data

With the calculation of the Co^{t}BuNC$^+$ ion heat of formation, we know the heats of formation of all of the products for the reaction

$$Co(CO)_2NO^tBuNC + h\nu \rightarrow Co^tBuNC^+ +$$
$$2CO + NO + e^- \quad (8)$$

This permits us to determine the heat of formation of the starting complex, Co(CO)$_2$NO^{t}BuNC, from the measured onset. Using the thermochemistry in Table 3, we obtain the 0 K neutral Co-(CO)$_2$NO^{t}BuNC heat of formation of -141 ± 10 kJ·mol^{-1}. From the derived heat of formation of the neutral molecule and its adiabatic ionization energy, we can determine the heats of formation of the molecular ion and all of the CO and NO loss product ions, which are listed in Table 3. One can find that the

molecular ion Co(CO)$_2$NO^{t}BuNC$^+$ has a heat of formation of 564 ± 11 kJ·mol^{-1}.

The above results can now be combined with previous measurements of the heats of formation of Co(CO)$_x$NO$^+$ ($x =$ 2,1,0)[19] and the Co$^+$ ion[60] in order to obtain Co^{t}BuNC bond energies. The derived bond energies are listed in Table 3 and Figure 5. Finally, we can use the heat of formation of neutral Co(CO)$_3$NO published earlier[19] to obtain the reaction enthalpy for the following reaction

$$Co(CO)_3NO + {}^tBuNC \rightarrow Co(CO)_2NO^tBuNC + CO$$
$$\Delta_r H \, (0 \text{ K}) = 32 \pm 13 \text{ kJ·mol}^{-1} \quad (9)$$

To convert the above thermochemical data to room temperature, one has to calculate $H°_{298} - H°_0$ values for the Co(CO)$_2$NO^{t}BuNC molecules and the various ions. The $H°_{298} - H°_0$ values obtained by using the B3LYP/6-31++G** frequencies are listed in Table 3 with the room temperature heats of formation of the neutral molecules and ionic species. Using these data along with the $H°_{298} - H°_0$ values of the elements (Co, 4.771 kJ·mol^{-1}; C, 1.051 kJ·mol^{-1}; N$_2$, 8.670 kJ·mol^{-1}; O$_2$, 8.683 kJ·mol^{-1}; P, 6.197 kJ·mol^{-1}; H$_2$, 8.468 kJ·mol^{-1}), the room temperature heats of formation for Co(CO)$_2$NO^{t}BuNC and its fragments can be calculated and are listed in Table 3. Throughout these calculations, the

*t*BuNC-Substituted Co(CO)₃NO

J. Phys. Chem. A, Vol. 111, No. 31, 2007 **7549**

Rosenstock (or ion) convention was used, in which the heat capacity of an electron is treated as 0.0 kJ·mol^{-1} at all temperatures.[60]

Conclusion

The electronic structure of the neutral Co(CO)₂NO*t*BuNC, the bond energies in the various fragment ions, and the thermochemistry of the Co(CO)₂NO*t*BuNC system have been determined by ultraviolet photoelectron spectroscopy (UPS), threshold photoelectron photoion coincidence spectroscopy (TPEPICO), and quantum chemical calculations.

The UPS study revealed that the *t*BuNC ligand is a better electron donor than the carbonyl group, increasing the electron density on the metal center and consequently lowering the vertical ionization energy of the molecule to 7.65 eV. By comparison of the *t*BuNC-substituted complex to earlier results on phosphine-substituted complexes, the electron donor strength of the *t*BuNC ligand was found to be between that of PEt₃ and PPr₃. Correlation was found between the vertical ionization energies and the Co−CO bond energies.

The adiabatic ionization energy of the molecule was found to be 7.30 ± 0.05 eV. The 0 K appearance energies of the various fragment ions (Co(CO)$_x$NO$_y$*t*BuNC$^+$, x = 2,1,0; y = 1,0) were determined from the analysis of the TPEPICO experiments. The highest photon energy available in the TPEPICO instrument was insufficient to observe either bare Co$^+$ or *t*BuNC$^+$. The heat of formation of the Co*t*BuNC$^+$ ion was estimated by carrying out ab initio and DFT calculations on the CoL$^+$ + *t*BuNC → Co*t*BuNC$^+$ + L (L = CO, NO, NH₃, PMe₃, H₂O) substitution enthalpies. On the basis of the statistics of the derived heats of formation, an uncertainty of 8.7 kJ·mol^{-1} was assigned to the value 1002.7 kJ·mol^{-1}. As a result, it is possible to combine this heat of formation with the appearance energies of the fragment ions to determine their heats of formation.

Supporting Information Available: The calculated (B3LYP/6-31++G**) harmonic vibrational frequencies required for the data analysis (Table 1), the substitution energies obtained in the DFT and ab initio calculations. (Table 2), the ZPE of the ionic complexes and the free ligands (Table 3), the detailed description of the TPEPICO data analysis with the RRKM-calculated rate constants of the three dissociation reactions from Co(CO)₂NO*t*BuNC$^+$ (Figure 1), and the sample ion internal energy distribution curves of the Co(CO)$_x$NO*t*BuNC$^+$ (x = 2,1,0) species (Figure 2). This material is available free of charge via the Internet at http://pubs.acs.org.

References and Notes

(1) Boese, R.; van Sickle, A. P.; Vollhardt, K. P. *Synthesis* **1994**, 1374.
(2) Lenges, C. P.; Brookhart, M.; Grant, B. E. *J. Organomet. Chem.* **1997**, *528*, 199.
(3) Pamplin, C. B.; Legzdins, P. *Acc. Chem. Res.* **2003**, *36*, 223.
(4) Lene, P. A.; Oliver, P. E.; Wright, P. J.; Reeves, C. L.; Piit, A. D.; Cockayne, B. *Chem. Vap. Deposition* **1998**, *4*, 183.
(5) Ivanova, A. R.; Nuesca, G.; Chen, X.; Goldberg, C.; Kaloyeros, A. E.; Arkles, B.; Sullivan, J. J. *J. Electrochem. Soc.* **1999**, *146*, 2139.

(6) Smart, C. J.; Reynolds, S. K.; Stanis, C. L.; Patil, A.; Kirleis, J. T. *Mater. Res. Soc. Symp. Proc.* **1993**, *282*, 229.
(7) Londergan, A. R.; Nuesca, G.; Goldberg, C.; Peterson, G.; Kaloyeros, A. E.; Arkles, B.; Sullivan, J. J. *J. Electrochem. Soc.* **2001**, *148*, C21.
(8) West, G. A.; Beeson, K. W. U.S. Patent 4814294, 1989.
(9) Crawford, N. R. M.; Knutsen, J. S.; Yang, K.; Haugstad, G.; McKernan, S.; McCormick, F. B.; Gladfelter, W. L. *Chem. Vap. Deposition* **1998**, *4*, 181.
(10) Hess, K. L.; Zehr, S. W. U.S. Patent 5045496, 1991.
(11) Hess, K. L.; Zehr, S. W.; Cheng, W. H.; Pooladdej, J.; Buehring, K. D.; Wolf, D. L. *J. Cryst. Growth* **1988**, *93*, 576.
(12) Dickson, R. S.; Yin, P.; Ke, M.; Johnson, J.; Deacon, G. B. *Polyhedron* **1996**, *15*, 2237.
(13) Sztáray, B.; Baer, T. *J. Am. Chem. Soc.* **2000**, *122*, 9219.
(14) Sztáray, B.; Szepes, L.; Baer, T. *J. Phys. Chem. A* **2003**, *107*, 9486.
(15) Li, Y.; Sztáray, B.; Baer, T. *J. Am. Chem. Soc.* **2001**, *123*, 9388.
(16) Li, Y.; Sztáray, B.; Baer, T. *J. Am. Chem. Soc.* **2002**, *124*, 4487.
(17) Li, Y.; Sztáray, B.; Baer, T. *J. Am. Chem. Soc.* **2002**, *124*, 5843.
(18) Li, Y.; Sztáray, B. *J. Phys Chem. A* **2002**, *106*, 9820.
(19) Sztáray, B.; Baer, T. *J. Phys. Chem. A* **2002**, *106*, 8046.
(20) Gengeliczki, Zs.; Sztáray, B.; Baer, T.; Iceman, C.; Armentrout, P. B. *J. Am. Chem. Soc.* **2005**, *127*, 9393.
(21) Révész, Á.; Pongor, Cs. I.; Bodi, A.; Sztáray, B.; Baer, T. *Organometallics* **2006**, *25*, 6061.
(22) Thorsteinson, E. M.; Basolo, F. *J. Am. Chem. Soc.*, **1966**, *88*, 3930.
(23) Csákvári, B.; Nagy, A.; Zanathy, L.; Szepes, L. *Magy. Kem. Foly.* **1992**, *98*, 415.
(24) Baer, T.; Booze, J. A.; Weitzel, K. M. Photoelectron Photoion Coincidence Studies of Ion Dissociation Dynamics. In *Vacuum Ultraviolet Photoionization and Photodissociation of Molecules and Clusters*; Ng, C. Y., Ed.; World Scientific: Singapore, 1991; p 259
(25) Baer, T.; Li, Y. *Int. J. Mass Spectr.* **2002**, *219*, 381.
(26) Sztáray, B.; Baer, T. *Rev. Sci. Instrum.* **2003**, *74*, 3763.
(27) Baerends, E. J.; Gritsenko, O. V. *J. Phys. Chem. A* **1997**, *101*, 5383.
(28) Chong, D. P.; Gritsenko, O. V.; Baerends, E. J. *J. Chem. Phys.* **2002**, *116*, 1760.
(29) Gritsenko, O. V.; Baerends, E. J. *J. Chem. Phys.* **2002**, *117*, 9154,
(30) Gritsenko, O. V.; Braïda, B.; Baerends, E. J. *J. Chem. Phys.* **2003**, *119*, 1397.
(31) Gritsenko, O. V.; Baerends, E. J. *J. Chem. Phys.* **2004**, *120*, 8364.
(32) Politzer, P.; Abu-Awwad, F. *Theor. Chem. Acc.* **1998**, *94*, 83.
(33) Gengeliczki, Zs.; Bodi, A.; Sztáray, B. *J. Phys. Chem. A* **2004**, *108*, 9957.
(34) Gengeliczki, Zs.; Pongor, Cs. I.; Sztáray, B. *Organometallics* **2006**, *25*, 2553.
(35) Becke, A. D. *J. Chem. Phys.* **1993**, *98*, 5648.
(36) (a) Lee, C.; Yang, W.; Parr, R. G. *Phys. Rev. B* **1988**, *37*, 785. (b) Miehlich, B.; Savin, A.; Stoll, H.; Preuss, H. *Chem. Phys. Lett.* **1989**, *157*, 200.
(37) (a) Schaefer, A.; Horn, H.; Ahlrichs, R. *J. Chem. Phys.* **1992**, *97*, 2571. (b) Schaefer, A.; Huber, C.; Ahlrichs, R. *J. Chem. Phys.* **1994**, *100*, 5829.
(38) Petersson, G. A.; Al-Laham, M. A. *J. Chem. Phys.* **1991**, *94*, 6081.
(39) (a) Hay, P. J.; Wadt, W. R. *J. Chem. Phys.* **1985**, *82*, 270. (b) Wadt, W. R.; Hay, P. J. *J. Chem. Phys.* **1985**, *82*, 284. (c) Hay, P. J.; Wadt, W. R. *J. Chem. Phys.* **1985**, *82*, 299.
(40) Bodi, A.; Sztáray, B.; Baer, T. *Phys. Chem. Chem. Phys.* **2006**, *8*, 613.
(41) Kercher, J. P.; Gengeliczki, Zs.; Sztáray, B.; Baer, T. *J. Phys. Chem. A* **2007**, *111*, 16.
(42) Wachers, A. J. H. *J. Chem. Phys.* **1970**, *52*, 1033.
(43) Hay, P. J. *J. Chem. Phys.* **1977**, *66*, 4377.
(44) Raghavachari, K.; Trucks, G. W. *J. Chem. Phys.* **1989**, *91*, 1062.
(45) Hurley, M. M.; Pacios, L. F.; Christiansen, P. A.; Ross, R. B.; Ermler, W. C. *J. Chem. Phys.* **1986**, *84*, 6840.
(46) (a) *Basis Set Exchange*; developed by the Collaboratory for Multiscale Chemical Science (CMCS) in cooperation with EMSL; operated and maintained by EMSL, Pacific Northwest National Laboratory (PNNL): Richland, WA. (b) *EMSL Basis Set Library*; maintained by EMSL, Pacific Northwest National Laboratory: Richland, WA.
(47) Kendall, R. A.; Dunning, T. H., Jr.; Harrison, R. J. *J. Chem. Phys.* **1992**, *96*, 6796.
(48) Seeger, R.; Pople, J. A. *J. Chem. Phys.* **1977**, *66*.
(49) Bauernschmitt, R.; Ahlrichs, R. *J. Chem. Phys.* **1996**, *104*, 9047.
(50) (a) Head-Gordon, M.; Pople, J. A.; Frisch, M. J. *Chem. Phys. Lett.* **1988**, *153*, 503. (b) Frisch, M. J.; Head-Gordon, M.; Pople, J. A. *Chem. Phys. Lett.* **1990**, *166*, 275. (c) Frisch, M. J.; Head-Gordon, M.; Pople, J. A. *Chem. Phys. Lett.* **1990**, *166*, 281. (d) Head-Gordon, M.; Head-Gordon, T. *Chem. Phys. Lett.* **1994**, *220*, 122. (e) Saebo, S.; Almlof, J. *Chem. Phys. Lett.* **1989**, *154*, 83.
(51) (a) Cizek, J. *Adv. Chem. Phys.* **1969**, *14*, 35. (b) Purvis, G. D.; Bartlett, R. J. *J. Chem. Phys.* **1982**, *76*, 1910. (c) Scuseria, G. E.; Janssen,

C. L.; Schaefer, H. F., III. *J. Chem. Phys.* **1988**, *89*, 7382. (d) Scuseria, G. E.; Schaefer, H. F., III. *J. Chem. Phys.* **1989**, *90*, 3700. (e) Pople, J. A.; Head-Gordon, M.; Raghavachari, K. *J. Chem. Phys.* **1987**, *87*, 5968.

(52) Frisch, M. J.; Trucks, G. W.; Schlegel, H. B.; Scuseria, G. E.; Robb, M. A.; Cheeseman, J. R.; Montgomery, J. A., Jr.; Vreven, T.; Kudin, K. N.; Burant, J. C.; Millam, J. M.; Iyengar, S. S.; Tomasi, J.; Barone, V.; Mennucci, B.; Cossi, M.; Scalmani, G.; Rega, N.; Petersson, G. A.; Nakatsuji, H.; Hada, M.; Ehara, M.; Toyota, K.; Fukuda, R.; Hasegawa, J.; Ishida, M.; Nakajima, T.; Honda, Y.; Kitao, O.; Nakai, H.; Klene, M.; Li, X.; Knox, J. E.; Hratchian, H. P.; Cross, J. B.; Bakken, V.; Adamo, C.; Jaramillo, J.; Gomperts, R.; Stratmann, R. E.; Yazyev, O.; Austin, A. J.; Cammi, R.; Pomelli, C.; Ochterski, J. W.; Ayala, P. Y.; Morokuma, K.; Voth, G. A.; Salvador, P.; Dannenberg, J. J.; Zakrzewski, V. G.; Dapprich, S.; Daniels, A. D.; Strain, M. C.; Farkas, O.; Malick, D. K.; Rabuck, A. D.; Raghavachari, K.; Foresman, J. B.; Ortiz, J. V.; Cui, Q.; Baboul, A. G.; Clifford, S.; Cioslowski, J.; Stefanov, B. B.; Liu, G.; Liashenko, A.; Piskorz, P.; Komaromi, I.; Martin, R. L.; Fox, D. J.; Keith, T.; Al-Laham, M. A.; Peng, C. Y.; Nanayakkara, A.; Challacombe, M.; Gill, P. M. W.; Johnson, B.; Chen, W.; Wong, M. W.; Gonzalez, C.; Pople, J. A. *Gaussian 03*, revision B.04; Gaussian, Inc.: Wallingford, CT, 2004.

(53) Frisch, M. J.; Trucks, G. W.; Schlegel, H. B.; Scuseria, G. E.; Robb, M. A.; Cheeseman, J. R.; Montgomery, J. A., Jr.; Vreven, T.; Kudin, K. N.; Burant, J. C.; Millam, J. M.; Iyengar, S. S.; Tomasi, J.; Barone, V.; Mennucci, B.; Cossi, M.; Scalmani, G.; Rega, N.; Petersson, G. A.; Nakatsuji, H.; Hada, M.; Ehara, M.; Toyota, K.; Fukuda, R.; Hasegawa, J.; Ishida, M.; Nakajima, T.; Honda, Y.; Kitao, O.; Nakai, H.; Klene, M.; Li, X.; Knox, J. E.; Hratchian, H. P.; Cross, J. B.; Bakken, V.; Adamo, C.; Jaramillo, J.; Gomperts, R.; Stratmann, R. E.; Yazyev, O.; Austin, A. J.; Cammi, R.; Pomelli, C.; Ochterski, J. W.; Ayala, P. Y.; Morokuma, K.; Voth, G. A.; Salvador, P.; Dannenberg, J. J.; Zakrzewski, V. G.; Dapprich, S.; Daniels, A. D.; Strain, M. C.; Farkas, O.; Malick, D. K.; Rabuck, A. D.; Raghavachari, K.; Foresman, J. B.; Ortiz, J. V.; Cui, Q.; Baboul, A. G.; Clifford, S.; Cioslowski, J.; Stefanov, B. B.; Liu, G.; Liashenko, A.; Piskorz, P.; Komaromi, I.; Martin, R. L.; Fox, D. J.; Keith, T.; Al-Laham, M. A.; Peng, C. Y.; Nanayakkara, A.; Challacombe, M.; Gill, P. M. W.; Johnson, B.; Chen, W.; Wong, M. W.; Gonzalez, C.; Pople, J. A. *Gaussian 03*, revision D.01; Gaussian, Inc.: Wallingford, CT, 2004.

(54) Hillier, I. H.; Guest, M. F.; Higginson, B. R.; Lloyd, D. R. *Mol. Phys.* **1974**, *27*, 215.

(55) Bursten, B. E.; Jense, R.; Gordon, J. G.; Treichel, P. M.; Fenske, R. F. *J. Am. Chem. Soc.* **1981**, *103*, 5226.

(56) Decleva, P.; Fronzoni, G.; De Alti, G.; Lisini, A. *J. Mol. Struct.: THEOCHEM* **1991**, *226*, 265.

(57) (a) Kassel, L. S. *J. Phys. Chem.* **1928**, *32*, 225. (b) Marcus, R. A.; Rice, O. K. *J. Phys. Colloid Chem.* **1951**, *55*, 894. (c) Rice, O. K.; Ramsperger, H. C. *J. Am. Chem. Soc.* **1927**, *49*, 1617.

(58) Gilbert, R. G.; Smith, S. C. *Theory of Unimolecular and Recombination Reactions*; Blackwell Scientific: London, U.K., 1990.

(59) Koizumi, H.; Baer, T. *J. Phys. Chem. A* **2004**, *108*, 5956.

(60) Chase, M. W. *J. Phys. Chem. Ref. Data, Mono.* **1998**, *9*.

(61) Cox, J. D.; Wagman, D. D.; Medvedev, V. A. *CODATA Key Values for Thermodynamics*; John Benjamins Publishing: New York, 1988.

(62) Walter, D.; Armentrout, P. B. *J. Am. Chem. Soc.* **1998**, *120*, 3176.

(63) Dalleska, N. F.; Honma, K.; Sunderlin, L. S.; Armentrout, P. B. *J. Am. Chem. Soc.* **1994**, *116*, 3519.